Appl Phys A (2010) 101: 237–241
DOI 10.1007/s00339-010-5807-9

Applied Physics A
Materials Science & Processing

Large-area micro/nanostructures fabrication in quartz by laser interference lithography and dry etching

C.H. Liu · M.H. Hong · M.C. Lum · H. Flotow ·
F. Ghadessy · J.B. Zhang

Received: 18 November 2009 / Accepted: 10 May 2010 / Published online: 10 June 2010
© Springer-Verlag 2010

Abstract Laser interference lithography (LIL) has the capability to fabricate large-area microstructures on the photoresist with only a couple of minutes' exposure and development. In this study, LIL was adopted to fabricate micro/nanostructures in quartz by combining the following dry-etching process either reactive ion etching (RIE) or inductively coupled plasma (ICP). A layer of gold film was coated on the quartz to act as a hard mask during the dry-etching process. A microhole array in quartz with a thin gold film covered on the surface was fabricated when choosing RIE. Each hole in the microhole array was surrounded with gold nanoparticle capped silica (Au/SiO_2) cones when using ICP instead of RIE. This is due to the thin gold film that serves as the mask for creating the surface roughness required for creating the silica cone structure.

1 Introduction

Over the past decades, two-dimensional micropatterned surfaces with desired morphology and surface property have attracted considerable attention and led to a wide range of applications in self-assembled biochemical sensors, well controlled cellular microenvironments, and medical diagnostic microdevices [1, 2]. Several approaches have been proposed to prepare patterned surfaces as self-assembly templates [3, 4], among which photolithography-based and soft-lithography-based techniques have been the most popular choices. In addition, high-aspect-ratio nanostructures, such as nanopillars, are becoming crucial for many novel applications, such as self-cleaning superhydrophobic coatings [5], dynamic wettability tuning for microfluidic manipulation [6], biomimetic dry adhesives [7], surface modification for biomolecule detection and cell studies [8], and so on. To fabricate the nanostructures with large aspect ratio, RIE is usually used together with metal masks with features in nanometer scale, which is typically fabricated using e-beam lithography [9, 10]. However, e-beam lithography is time-consuming and expensive, and, therefore, not suitable for the large-area fabrication of nanoscale structures for practical applications. Other methods such as polymer sphere lithography [11] and sedimentation of colloidal gold particles as etching masks [12] have been studied. However, they suffer from difficulty to form monolayer of closely packed nanospheres and sensitivity to contamination, respectively. A simple alternative is the self-formation of nanoscale etching masks in the form of rough metal films with an inevitable drawback of broad size distribution of fabricated nanostructures [13].

These studies focused on either microstructure or nanostructure fabrication with different techniques. In this study, we fabricated both micrometer and nanometer structures simultaneously by the dry-etching process. The microstructure is a periodical microhole array for micrometer bio-functional beads capture, and the nanostructure surrounds each microhole with the possibility to improve beads dispersing capability because of their wettability tuning to the substrate [6]. Considering the substrate, glass or quartz

C.H. Liu · M.H. Hong (✉)
Department of Electrical and Computer Engineering, National University of Singapore, 4 Engineering Drive 3, Singapore 117576, Singapore
e-mail: elehmh@nus.edu.sg

C.H. Liu · M.C. Lum · H. Flotow · F. Ghadessy
Experimental Therapeutics Center, ASTAR, 31 Biopolis Way Nanos Level 3, Singapore 138669, Singapore

M.H. Hong · J.B. Zhang
Data Storage Institute, 5 Engineering Drive 1, Singapore 117608, Singapore

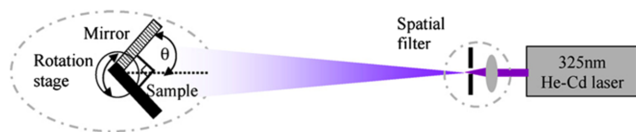

Fig. 1 The schematic diagram of a laser interference lithography setup

are conventional inorganic substrates, and widely used in bio-diagnostics and biomedical research because of their well-understood and adapted physical and chemical properties [14]. Here, we fabricated microhole array in quartz with Au film covered on the top surface through LIL and RIE processing. The hydrophobic property of the metal film would improve the chip capability for dispersing bio-functional beads. Moreover, we fabricated hybrid array structures of microhole with Au/silica nanocones surrounded through LIL and ICP processing. The high-aspect-ratio nanostructures would have better hydrophobic property compared to metal film. The LIL applied has the advantages of being non-contact process in air and maskless lithography at a high speed with low system investment for large-area pattern fabrication.

2 Experiment details

Laser interference lithography (LIL) is applied in micro/nanostructure fabrication. LIL is a maskless lithography technique, which makes use of the interference pattern of two incident laser beams and records the pattern on a photoresist material. LIL has also proven its ability to generate uniform two-dimensional patterns over a large area [15]. The interference pattern consists of a standing wave whose intensity varies with a period equal to $p = \lambda/(2\sin\theta)$, where λ is the wavelength of the laser beams, and θ the half angle at which two beams intersect. In this experiment, the exposure was carried out using Llyod's mirror setup [16] with a 325 nm helium–cadmium (He–Cd) continuous wave laser as the light source, as shown in Fig. 1.

Quartz substrate was first thoroughly washed with acetone, followed by isopropyl alcohol (IPA) solution, and finally by deionized (DI) water. A 50 nm Au film deposition was carried out using an electron beam evaporator, as shown in Fig. 2(a). Negative photoresist MAN1407 was spin-coated on the top of Au layer, followed by a prebake at 100°C for 1 min 30 sec. The spin-coating was done at 3500 rpm for 30 sec. The resulting photoresist has a thickness of around 700 nm, as shown in Fig. 2(b).The photoresist pattern was formed by LIL. The exposure laser power is around 0.2 mW and the exposure time used was 3 min. The angle θ was set according to the designed pattern dimension. Array of photoresist holes was achieved by rotating the sample by 90° and subjecting it to a second exposure, as shown in Fig. 2(c). Au etchant was adopted to

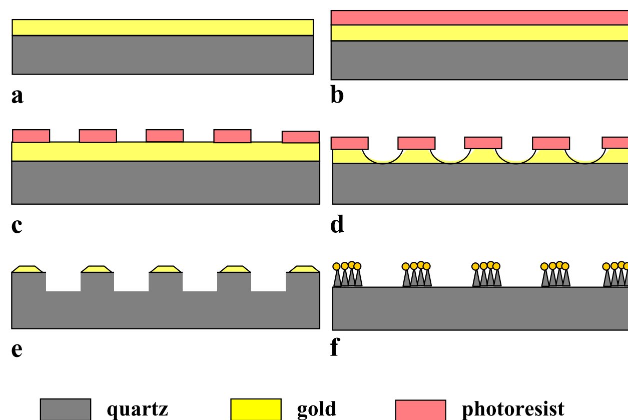

Fig. 2 Schematic diagram of experimental procedures: (**a**) 50 nm Au film coating on quartz substrate; (**b**) negative photoresist coating; (**c**) photoresist exposure by LIL and development; (**d**) Au etchant; (**e**) RIE or (**f**) ICP

etch away the exposed Au for deep holes. The wet chemical etchant creates anisotropic profiles, as shown in Fig. 2(d). After these processing, either RIE or ICP was chosen to fabricate the structures. The schematic diagram of the RIE result is shown in Fig. 2(e), which is Au covered on the top surface of the quartz microhole array. For the ICP result is shown in Fig. 2(f), which is Au/SiO_2 cones surrounded microhole array.

In the dry-etching process, the photoresist pattern was transferred to quartz substrate with photoresist and Au film as the mask. For RIE, the etching gas was CF_4 with a flow rate of 50 sccm (standard cubic centimeters per minute). The samples were etched for 15 min with 20 mTorr chamber pressure and 250 W etching power. After etching the samples were cleaned immediately with acetone to remove any residual reactive gas. When using ICP dry-etching process, the reactive ion etching chamber had a pressure of 5 mTorr. CF_4 gas was released into the chamber as an etchant at a flow rate of 50 sccm for 6 min. One power source (1000 W) was used to generate dense plasma from the input gases. A second power source (70 W) applied a voltage of approximately 600 V to accelerate the plasma toward the substrate. Both power sources operated at a frequency of 13.5 MHz. Helium gas also simultaneously flowed at the back of the substrate to maintain a temperature of 60°C during fabrication.

3 Results and discussion

Figures 3(a) and (b) show the imaging of the etched microhole array with Au film covered on the top surface of the structures, which were fabricated through LIL and RIE dry-etching process. An area of 5 mm × 5 mm microhole array was fabricated with around 6.2 million holes. The area

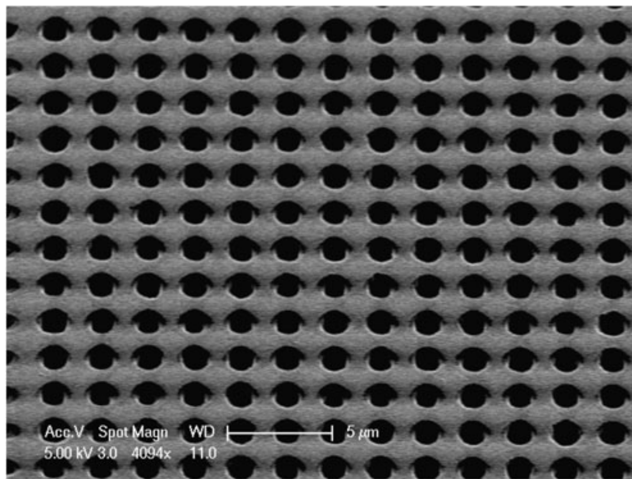

a

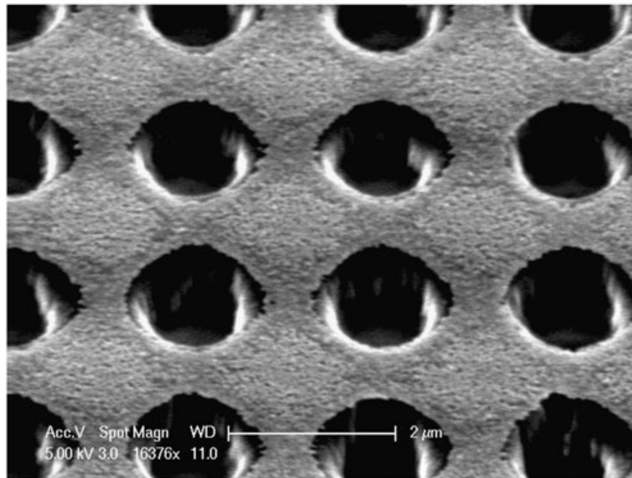

b

Fig. 3 (**a**), (**b**) SEM imagings of quartz microhole array with gold covered on the top surface of the array

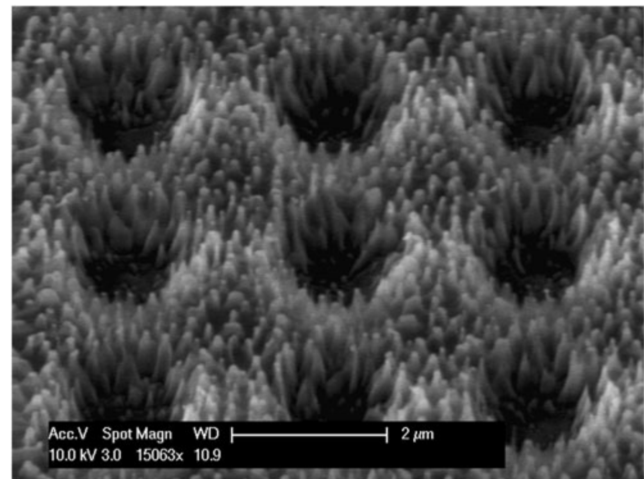

a

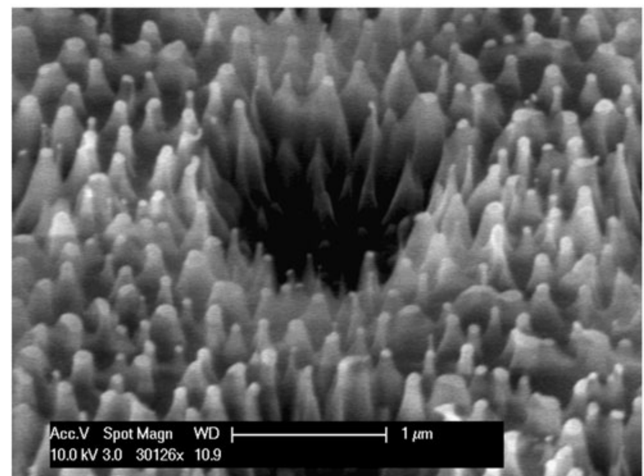

b

Fig. 4 (**a**), (**b**) SEM imagings of quartz microhole array surrounded by Au nanoparticle capped silica nanocones

can be increased with the same exposure time if a higher-power laser is applied. It can be seen that the diameter of the hole is around 1.2 µm and the space between holes is around 750 nm. The period can be tuning easily by changing θ, and the feature size can be controlled by the exposure time.

In the RIE process, CF_4 was chosen as the etching gas. It is commonly used as a chemical etchant for either RIE (or ICP) silicon (or silica) processing as fluorine radicals created in the plasma react easily with Si [17]. When the prepared sample as shown in Fig. 2(d) was undergoing the RIE process, the fluorine plasma-generated ions chemically reacted with the exposed quartz substrate directly. The etching rate could reach 100 nm/min under the setting parameters. At the same time, the use of plasma-generated ions is a pure physical ion bombardment process at the mask of photoresist and Au layer although there is no chemical reaction. The photoresist is around 700 nm and the originally coated Au film is around 50 nm. After 15 min RIE process, the photoresist was milled away completely while a few nanometers Au layer is left. It can be seen clearly in Fig. 3(b) that an Au thin film covers the top surface of the microholes, and there are also Au nanoparticles shown in the imaging.

According to the etch rate of fluorine with fused quartz, the hole depth should be around 1.5 µm after 15 min etching. However, the depth of the hole was measured to be around 1.1 µm. It is possibly due to the Au etching process did not etch away all the exposed Au completely. The plasma-generated ions have to physically knock off the Au thin film before chemically react with the quartz substrate. Therefore, the depth of the hole in experiment is less than the expected value.

Figures 4(a) and (b) show the imaging of Au nanoparticle capped silica (Au/SiO_2) cones surrounded microhole array. For the same prepared samples before RIE or ICP process by LIL and Au etching, the sample fabricated by ICP process has also the same pattern area, the same period and feature size. The hole depth is closely related with the dry-etching

parameters, such as etching power, gas flow rate and etching time. The hole depth in Fig. 4 is around 1 μm under the parameters described in experiment details.

ICP etch system typically contains two radio frequency (RF) power sources and each of these power sources introduces energy into the system in different ways. The ICP power introduces energy by the use of an RF induction coil upstream from the sample. This source does not couple its energy through the sample and can feed the chamber with large amounts of power without affecting the sample electrically. The second RF power source is the bias power which is located at the substrate holder. This source is needed to form a plasma potential and obtain an anisotropic etch. Plasma density and ion energy play important roles in ICP system, and they are controlled and determined by ICP power and bias power, respectively. ICP is a type of low-pressure and high-density plasma discharges compared with RIE which has the limitations of capacitive RF discharges and their magnetically enhanced variants. Therefore, ICP dry etching is a choice for small feature size etching process and provides anisotropic and directional etch [17].

At the beginning of the ICP dry-etching process, the photoresist were milled away rapidly and the thickness of Au film was reduced quickly resulting from the high density of physical ions bombardment. As we mentioned in Fig. 3(b), the Au film became only a few nanometer thickness with obvious Au nanoparticles in the SEM imaging. In ICP dry-etching process, the Au nanoparticles occurred earlier due to much higher-density ion bombardment. When the Au film became a thin layer of separated nanoparticles, they served as the mask for creating the silica nanocones. Since the Au nanoparticles were formed from ion bombardment, they have a broad size distribution. It can be seen from Fig. 4(b), the nanoparticle diameter ranges from 5 nm to 150 nm and the height of nanocone is around 1 μm. The aspect ratio (AR = height/diameter) of the nanostructures ranges from 200 to 7. The shape of silica nanocones varies with the different nanoparticle diameters. Meanwhile, the chemical etching of fluorine ions with quartz substrate was very efficient, which led to quite a deep hole during the process. By this approach, the hybrid micrometer and nanometer structure can be designed and fabricated to increase the bio-functional beads dispersion capability. The microstructure is determined by the LIL technique, which is quite flexible for the pattern size and shape tuning [18, 19]. The further size and structure design will be realized by flexibly tuning the parameters in LIL and also the ICP dry-etching parameters.

In addition, a 50 nm Au film coated quartz forms a rough surface by a wet etching process using Au etchant, and then SiO_2 etching process by ICP. The quartz surface imaging is shown in Fig. 5(a) and (b). It is a large-area Au nanoparticle capped silica nanocones. The Au nanoparticle diameter ranges from 5 nm to 80 nm, which is smaller than Fig. 4. It is possibly due to the directly wet etching on the Au film surface, which creates better surface roughness as a mask for dry etching. Using gold thin film or nanoparticles as a mask for high-aspect-ratio nanostructures fabrication has been studied in previous research. The presence of gold nanoparticles is actually controlled by etching parameters [20, 21]. For Au/SiO_2 nanocones, it is one of the catalyst candidates for CO oxidation with better thermal stability and easy regeneration property [22].

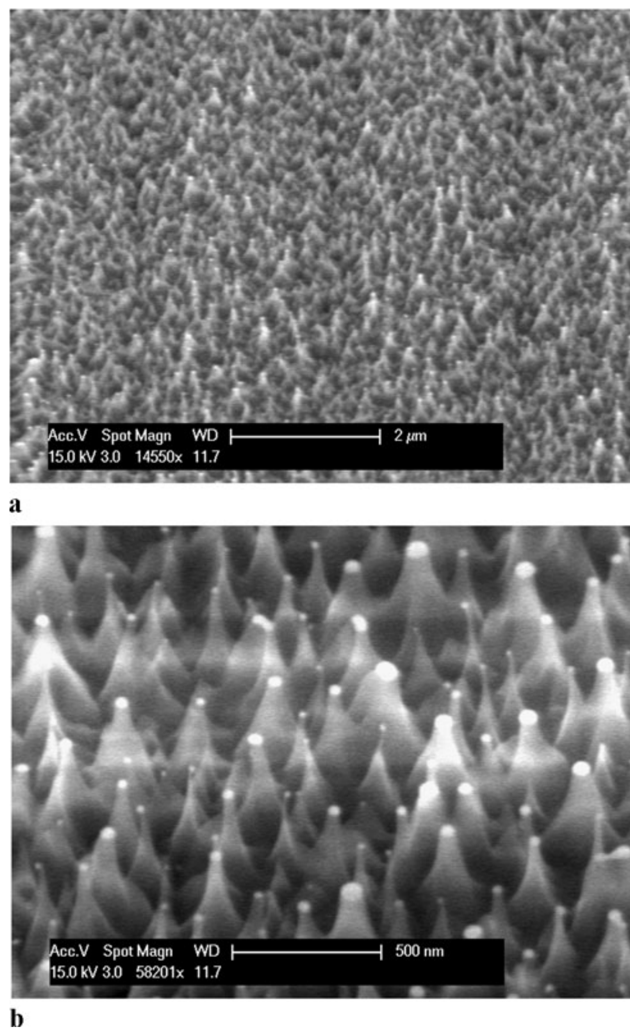

Fig. 5 (**a**), (**b**) SEM imagings of large-area Au capped silica nanocones

4 Conclusions

Micropatterned structures with desired surface property are quite important in biochemical and bio-diagnostic devices. Meanwhile, nanopatterned structures with high aspect ratio are capable of wettability tuning and surface modification for biomolecule detection and cell studies. In this study,

we fabricated microstructure and nanostructures simultaneously in quartz substrate for bio-functional beads dispersion. The periodical microstructure of microhole array is determined by laser interference lithography technique to tune the size and shape. By controlling the dry-etching process either RIE or ICP, the top surface of the microhole array can be flexibly formed as metal film with rough surface or Au nanoparticle capped silica nanocones. The nanostructures form owes to the gold film that serves as the mask for creating the surface roughness to create the silica nanocones when applying ICP dry etching process. The aspect ratio of silica cone could reach 200, although the nanocones' size is not uniform. The nanostructure was designed to modify the substrate surface by wettability tuning. Further research of the bio-functional beads dispersion and the structure dimension design are in progress.

Acknowledgement This work is supported by Singapore Agency for Science, Technology and Research (A* STAR) Cross Council Office Grant CCOG01_003_2008.

References

1. J. Aizenberg, A.J. Black, C.M. Whitesides, Nature **398**, 495 (1999)
2. Y. Cui, Q.Q. Wei, H.K. Park, C.M. Leiber, Science **293**, 1289 (2001)
3. X. Chen, Z. Chen, N. Fu, G. Lu, B. Yang, Adv. Mater. **15**, 1413 (2003)
4. G.M. Whitesides, B. Grzybowski, Science **295**, 2418 (2002)
5. W. Barthlott, C. Neinhuis, Planta **202**, 1 (1997)
6. T.N. Krupenkin, J.A. Taylot, T.M. Schneider, S. Yang, Langmuir **20**, 3824 (2004)
7. K. Autumn, Y.A. Liang, S.T. Hsieh, W. Zesch, W.P. Chan, T.W. Kenny, R. Fearing, R.J. Full, Nature **405**, 681 (2000)
8. K. Kuwabara, M. Ogino, S. Motowaki, A. Miyauchi, Microelectron. Eng. **73/74**, 752 (2004)
9. W. Chen, H. Ahmed, Appl. Phys. Lett. **62**, 1499 (1993)
10. A.P.G. Robinson, R.E. Palmer, T. Tada, T. Kanayama, M.T. Allen, J.A. Preece, K.D.M. Harris, J. Phys. D **32**, L75 (1999)
11. J.C. Hulteen, R.P. Van Duyne, J. Vac. Sci. Technol. A **13**(3), 1553 (1995)
12. P.A. Lewis, H. Ahmed, B.W. Alphenaar, Microelectron. Eng. **57/58**, 925 (2001)
13. K. Seeger, R.E. Palmer, Appl. Phys. Lett. **74**(11), 1627 (1999)
14. H. Cong, A. Revzin, T. Pan, Nanotechnology **20**, 075307 (2009)
15. M.L. Schattenburg, R.J. Aucoin, J. Vac. Sci. Technol. B **13**(6), 3007–3011 (1995)
16. S. Tolansky, *An Introduction to Interferometry* (Longmans, Green, New York, 1955)
17. M.A. Lieberman, A.J. Lichtenberg, *Principles of Plasma Discharges and Materials Processing*, 2nd edn. (Wiley, Hoboken, 2005)
18. W.K. Choi, T.H. Liew, M.K. Dawood, H.I. Smith, C.V. Thompson, M.H. Hong, Nano Lett. **8**(11), 3799–3802 (2008)
19. M.H. Hong, C.H. Liu, F. Ma, Z.C. Chen, B. Luk'yanchuk, L.P. Shi, T.C. Chong, Proc. SPIE **7202**, 72020K (2009)
20. J.R. Morber, X. Wang, J. Liu, R.L. Snyder, Z.L. Wang, Adv. Mater. **21**, 2072–2076 (2009)
21. S. Choi, H. Park, S. Lee, K.H. Koh, Thin Solid Films **513**, 31–35 (2006)
22. G.M. Veith, A.R. Lupini, S. Rashkeev, S.J. Pennycook, D.R. Mullins, V. Schwartz, C.A. Bridges, N.J. Dudney, J. Catal. **262**, 92–101 (2009)